Available online at www.sciencedirect.com

ScienceDirect

IFAC PapersOnline CONFERENCE PAPER ARCHIVE

IFAC PapersOnLine 51-29 (2018) 56–61

Articulating Parametric Nonlinearities in Computationally Efficient Hydrodynamic Models

Giuseppe Giorgi * **John V. Ringwood** **

* *(e-mail: giuseppe.giorgi.2015@mumail.ie)*
** *(e-mail: john.ringwood@mu.ie)*
Centre for Ocean Energy Research, Maynooth University, Ireland.

Abstract: Wave energy devices are designed, and controlled, in order to be extremely responsive to incoming wave excitation, hence maximising power absorption. Due to the consequent large motion excursions, highly nonlinear behaviour is likely to occur, especially in relation to variations in wetted surface. Moreover, nonlinearities may induce parametric instability, or activate internal mechanisms for exchanging energy between different degrees of freedom (DoFs), usually affecting the overall efficiency of the device. Consequently, single-DoF *linear* models may produce overly optimistic power production predictions, and neglect important dynamics of the system. One highly nonlinear phenomenon, particularly detrimental to power absorption for several wave energy converters, is parametric roll, which internally diverts part of the energy flow, from the axis where the power take-off is installed, to a secondary axis, generating parasitic motion. This paper proposes a computationally efficient multi-DoFs nonlinear model, which can effectively describe nonlinear behaviour, such as parametric pitch and roll, and their impact on motion prediction, power production assessment, and optimal control parameters.

Keywords: Nonlinear hydrodynamics, parametric resonance, parametric roll, wave energy converter, control, many-degrees-of-freedom systems.

1. INTRODUCTION

Linear models, although regularly used in the wave energy field, are prone to excessive optimism in motion prediction and power production assessment, and completely neglect purely nonlinear behaviour. Indeed, the conditions under which linear models are accurate (small relative motion between the device and the seawater) are seldom met, since the objective of a wave energy converter (WEC), pursued by the control strategy, is to maximise power absorption, by exaggerating the motion amplitude (Giorgi and Ringwood, 2017). Under such conditions, linear models perform poorly, losing accuracy and reliability, with important consequences, not only with regard to motion and power absorption prediction, but also in relation to the accuracy of model-based optimal control strategies. In particular, the effectiveness of the control strategy, on which the efficiency of the WEC is highly dependent, relies on the fidelity of the mathematical model the control is based on.

The accuracy of linear models may be improved by introducing relevant nonlinearities, which are dependent on the device dimensions and operating principle (Giorgi and Ringwood, 2018b). An effective solution for heaving point absorbers, which are small in dimension compared to the wave length, is the use of nonlinear Froude-Krylov (FK) models, where the *instantaneous* wetted surface is considered, as compared to the utilisation of the mean wetted surface for a linear model. One notable example of extremely nonlinear behaviour, which is undetected by linear models, but described by nonlinear FK models, is parametric pitch and roll motion. Parametric resonance is a phenomenon related to time variation in some system parameters, which may lead, under particular circumstances, to dynamic instability.

Particular examples, in the wave energy community, are given by the SEAREV (Babarit et al., 2009) and the Wavebob (Tarrant and Meskell, 2016) devices, for which parametric resonance is a detrimental, difficult to model and predict, parasitic effect. In fact, parametric instability is an internal excitation mechanism, which nonlinearly diverts part of the energy, from the axis where power is absorbed, to a secondary axis, ultimately causing significant efficiency erosion. For the SEAREV and Wavebob devices, parametric resonance was studied with mesh-based nonlinear FK force models (Gilloteaux, 2007), which compare well with wave tank tests, provided an appropriate viscous drag description is included. Nonetheless, the main drawback of mesh-based nonlinear FK models is the computational time, since they require time-consuming remeshing routines, which makes them slow, and not suitable for control or optimization applications.

However, a computationally efficient approach is proposed in this paper, applicable to axisymmetric devices. While previous work focused on single-body and single-degree of freedom (DoF) devices (Giorgi and Ringwood, 2017), this paper focuses on a multi-body multi-DoFs instead. A simple self-reacting point absorber, inspired by the Wavebob device, is considered, and modelled in all its degrees of

2405-8963
Peer review under responsibility of International Federation of Automatic Control.
10.1016/j.ifacol.2018.09.469

freedom. Despite the simplicity of the geometry, significant differences are found, between the linear and nonlinear model, with important consequences for optimization of the control parameters. Moreover, parametric roll is clearly evident and articulated, and its dependence on the power-take off (PTO) is discussed.

The remainder of the paper is organized as follows: Sect. 2 presents the linear and nonlinear mathematical models, while Sect. 3 describes the device configuration and parameters, and the wave conditions analyzed. Some results are presented in Sect. 4, while Sect. 5 gives concluding remarks and considerations.

2. MATHEMATICAL MODEL

Two right-handed frames of reference are introduced: an inertial frame (x, y, z), with the origin at the still water level (SWL), x pointing in the direction of propagation of the wave, and z pointing upwards; and a non-inertial frame $(\hat{x}, \hat{y}, \hat{z})$, fixed with the body, and overlapping with the inertial frame when the body is at rest. Under the hypothesis of an inviscid fluid, and irrotational and incompressible flow, linear potential theory can be formulated, defining the equation of motion for a generic single-body, in the body-fixed frame of reference, as:

$$M\ddot{\mathbf{x}} = \mathbf{f}_{FK_{st}} + \mathbf{f}_{FK_{dy}} + \mathbf{f}_{d} + \mathbf{f}_{rad} + \mathbf{f}_{vis} + \mathbf{f}_{Cor} + \mathbf{f}_{moor} + \mathbf{f}_{PTO}, \tag{1}$$

where M is the inertial matrix, $\mathbf{x} = (\hat{x}, \hat{y}, \hat{z}, \phi, \theta, \psi)$ is the state vector in the body-fixed frame, $\mathbf{f}$ are the generalized force vectors, composed of 3 forces ($\mathbf{F}$), and 3 torques ($\mathbf{T}$). The force components on the right hand side of (1) are the static and dynamic FK forces $\mathbf{f}_{FK_{st}}$ and $\mathbf{f}_{FK_{dy}}$, respectively, the diffraction force $\mathbf{f}_{d}$, the radiation force $\mathbf{f}_{rad}$, the viscous force $\mathbf{f}_{vis}$, the Coriolis force $\mathbf{f}_{Cor}$, the mooring force $\mathbf{f}_{moor}$, and the PTO force $\mathbf{f}_{PTO}$.

The mooring system is potentially an important factor for the generation of parametric instability, according to the particular mooring configuration (Davidson and Ringwood, 2017). Likewise, the viscous drag force, normally modelled as a Morison-like term (Bhinder et al., 2011), may be essential in nonlinear FK force models, to avoid an unrealistic magnification of the motion when parametric instability appears (Babarit et al., 2009). In this paper, linear radiation and diffraction forces have been considered, which is a reasonable approximation for devices much smaller than the characteristic wave length (Falnes, 2002). A computationally convenient state space representation has been used to model radiation forces, based on a moment-matching technique (Faedo et al., 2017).

Froude-Krylov forces correspond to the integral of the pressure of the undisturbed incident wave field, over the wetted surface of the device. Such a pressure is defined, according to linear Airy's theory, as:

$$p(x, z, t) = p_{st} + p_{dy} = -\gamma z + \gamma \frac{\cosh\left(k\left(z + h\right)\right)}{\cosh\left(kh\right)} \eta(x, t) \tag{2}$$

where $p_{st} = -\gamma z$ is the static pressure, p_{dy} the dynamic pressure, γ the specific weight of sea water, $\eta(x, t)$ a 2-dimensional wave with amplitude a and wave frequency ω, k the wave number, and h the water depth. It is also convenient to apply Wheeler stretching to (2), as shown in (Giorgi and Ringwood, 2018c).

Froude-Krylov forces ($\mathbf{F}_{FK}$) and torques ($\mathbf{T}_{FK}$) are computed by integrating the pressure, shown in (2), over the instantaneous wetted surface $S(t)$:

$$\mathbf{F}_{FK_{st}} + \mathbf{F}_{FK_{dy}} = \mathbf{F}_{g} + \iint_{S(t)} p_{st}\mathbf{n}dS + \iint_{S(t)} p_{dy}\mathbf{n}dS \tag{3a}$$

$$\mathbf{T}_{FK_{st}} + \mathbf{T}_{FK_{dy}} = \mathbf{r}\times\mathbf{F}_{g} + \iint_{S(t)} p_{st}\mathbf{r}\times\mathbf{n}dS + \iint_{S(t)} p_{dy}\mathbf{r}\times\mathbf{n}dS \tag{3b}$$

where $\mathbf{F}_{g}$ is the gravity force, $\mathbf{n} = (n_x, n_y, n_z)$ is the unit vector normal to the surface, pointing outwards, $\mathbf{r}$ is the position vector, and $\times$ is the cross product.

Under linear approximation, a constant wetted surface is considered, in integrals (3a) and (3b), relying on the assumption of small relative motion between the wave and the device. In contrast, nonlinear FK forces are computed with respect to the *instantaneous* wetted surface, therefore taking the real position of the device, with respect to η, into account.

For a geometry of arbitrary complexity, the actual calculation of the nonlinear FK integrals requires the use of plane panels to discretize the surface, which consequently has to be remeshed, at every time step, in order to define the instantaneous wetted surface (Gilloteaux, 2007). Such a remeshing routine makes the approach computationally expensive. However, for *axisymmetric* buoys, a convenient parametrization of the wetted surface can ease the calculation of the FK integrals. Such a method, described hereafter, is validated in (Giorgi and Ringwood, 2018b).

The assumption of axisymmetric geometry allows an analytical description of the whole wetted surface. The geometry of a generic buoy, symmetric around a vertical axis, can be described in cylindrical coordinates, with respect to the body-frame $(\hat{x}, \hat{y}, \hat{z})$, as follows:

$$\begin{cases} \hat{x}(\varrho, \vartheta) = f(\varrho)\cos\vartheta \\ \hat{y}(\varrho, \vartheta) = f(\varrho)\sin\vartheta \\ \hat{z}(\varrho, \vartheta) = \varrho \end{cases}, \quad \theta \in [-\pi, \pi) \wedge \varrho \in [\varrho_1, \varrho_2] \tag{4}$$

where $f(\vartheta)$ is a generic function of the vertical coordinate ϱ, describing the profile of revolution of the axisymmetric body, as shown in (Giorgi and Ringwood, 2017).

The change of coordinates, from Cartesian $(\hat{x}, \hat{y}, \hat{z})$ to cylindrical (ϱ, ϑ), shown in (4), requires the inclusion of $\|\mathbf{e}_{\varrho} \times \mathbf{e}_{\vartheta}\|$ in the integral, where $\mathbf{e}_{\varrho}$ and $\mathbf{e}_{\vartheta}$ are unity vectors in the ϱ and ϑ directions, respectively. Furthermore, $\mathbf{n}$ can be expressed as $\frac{\mathbf{e}_{\varrho}\times\mathbf{e}_{\vartheta}}{\|\mathbf{e}_{\varrho}\times\mathbf{e}_{\vartheta}\|}$. Finally, since the integrals are defined in the body frame, it is necessary to map the pressure from the inertial-frame (where it is defined) onto the body surface. The transformation, from (x, y, z) to $(\hat{x}, \hat{y}, \hat{z})$, is represented by the Euler angle triad (ϕ, θ, ψ), corresponding to roll, pitch, and yaw angles, respectively.

The 3-2-1 Euler angle sequence is the rotation convention commonly used for marine vehicles, thought of as three sets of rigid rotations Fossen (2011). Consequently, the integral for $\mathbf{F}_{FK_{dy}}$ in (3a), for example, becomes:

$$\mathbf{F}_{FK_{dy}} = \iint_{S(t)} p_{dy}(\hat{x},\hat{y},\hat{z})\mathbf{n}dS = \int_{\vartheta_1}^{\vartheta_2}\int_{\varrho_1}^{\varrho_2} p_{dy}(\varrho,\vartheta)\,(\mathbf{e}_\varrho \times \mathbf{e}_\vartheta)\,d\varrho d\vartheta \tag{5}$$

Although such an approach is applicable to any geometry with revolution symmetry, the vast majority of axisymmetric point absorbers can be described as a combination of cylinders, cones, and spheres. Note that discs (lids), which close the surface of a cylinder, cannot be described using cylindrical coordinates. To this end, polar coordinates are valid alternatives to cylindrical, as shown in (Giorgi and Ringwood, 2018b).

Finally, the FK force integrals must be solved numerically using, for example, a trapezoidal rule. The computation time depends on the integration scheme utilized, and on the relative and absolute tolerances used to approximate the integral, which have been set to 10^{-3} and 10^{-1}, respectively. The ultimate value of the computation time depends on the hardware capabilities, on the complexity of the geometry, and on the number of bodies/DoFs considered. For the device studied in this paper, described in Sect. 3, the calculation time of the nonlinear FK forces, in 7-DoFs, for two bodies, is between $1 \cdot 10^{-2}s$ and $5 \cdot 10^{-2}s$, at a single time instant. The consequent run time for computing the response of the device depends on the discrete time solver scheme, the time step, and the simulation duration. Using a constant time step Runge-Kutta scheme, varying the time step from $0.01s$ to $0.08s$, for wave periods of about $3s$, the resulting run time is between one and three times the simulation time. Therefore, such a method has the potential to run roughly in real time, or a little slower, depending on the particular implementation. However, these considerations are for computations performed in Matlab, which is between one and two orders of magnitude slower than lower level coding languages, such as C or Fortran (Wendt et al., 2017). With C or Fortran implementation, therefore, real time execution is easily achievable.

3. CASE STUDY

A simplified version of the Wavebob device, at 1:17 prototype scale, is considered as a case study, since Tarrant and Meskell (2016) demonstrate, through tank tests and a mesh-based nonlinear FK model, peculiar parametric instability for the Wavebob device, with negative consequences on the efficiency. The slightly simplified Wavebob-like WEC is a self-reacting heaving device, with a cylindrical spar (radius $0.3m$, draft $3.5m$), moving inside a cylindrical torus (outer radius $0.62m$, inner radius $0.36m$, draft $0.35m$). Since the real Wavebob device has a ballast system at the bottom of the spar, it has been assumed that two thirds of the weight of the spar is uniformly distributed in the bottom half of it. The centre of gravity and inertia properties are computed accordingly. A linear mooring system is considered attached to the spar. The PTO, which acts between the two bodies, extracting energy from the relative heave motion, is modelled as a linear damper. Finally, as in (Tarrant and Meskell, 2016), the 12 DoFs (6 DoFs for each body) are reduced to 7, considering heave for both bodies ($\hat{z}_s$ and $\hat{z}_t$, respectively for the spar and the torus), and the remaining five DoFs (surge $\hat{x}$, sway $\hat{y}$, roll ϕ, pitch θ, and roll ψ) for the whole system, considered as a single body. Note that, for simulations, a small initial roll and pitch angle position (0.007rad) has been employed, as suggested by Tarrant and Meskell (2016), in order to provide some initial energy in such DoFs. If not excited, either internally or externally, such small angles quickly decrease to zero; conversely, the roll angle increases only when parametric resonance occur.

The geometry has been simplified because of the intention to study mainly those nonlinearities related to pitch and roll motion. In fact, if the cylinder and cylindrical torus were to be constrained to a purely heaving motion, their response would be essentially linear, due to their constant cross sectional area (Penalba et al., 2017). Conversely, when large pitch/roll angles appear, even such geometries are subject to nonlinearities in the FK forces.

The choice of a self-reacting type of device is driven by the fact that such devices are particularly prone to parametric resonance, which is a Mathieu-type of instability (Fossen and Nijmeijer, 2012), caused by time-varying system parameters. In the case of the considered WEC, the leading causes of parametric instability are the variation of the metacentre, and of centre of gravity, due to pitch and relative heave motion, and to variations in wetted surface. Furthermore, the Mathieu-type of instability is well-known to appear, after a certain wave amplitude threshold, at an exciting frequency twice the pitch natural frequency (Fossen and Nijmeijer, 2012). Due to the typical long spar of a system like the Wavebob, the pitch natural frequency is usually low. Consequently, some of the wave excitation frequencies normally experienced in nominal power production conditions are likely to be twice the pitch natural period, meeting the frequency requirement of the Mathieu equation.

However, for a fully coupled nonlinear 7-DoF model, the notion of a single natural frequency in pitch is quite blurred, as explained in (Tarrant and Meskell, 2016; Giorgi and Ringwood, 2016), making the condition on the frequency less meaningful. Furthermore, the Mathieu equation is defined for single DoF unforced dynamic equation, with harmonic variations of the stiffness term, i.e. there is no true coupling between DoFs. Although it can give some insight, it cannot forecast the severity of the eventual parametric response. Moreover, various approximations are necessary to squeeze the nonlinear multi-DoF model into the single-DoF, partially linearized, model required by the Mathieu equation (Giorgi and Ringwood, 2018a).

Nevertheless, as shown in (Tarrant and Meskell, 2016), parametric instability is a frequency dependent phenomenon. Therefore, as is commonplace in the literature concerning parametric resonance, regular waves are primarily considered, to give frequency-resolved insight. Given the threshold condition, parametric roll also depends on wave amplitude. Since FK nonlinearities mainly depend on wave steepness, defined as the ratio between the

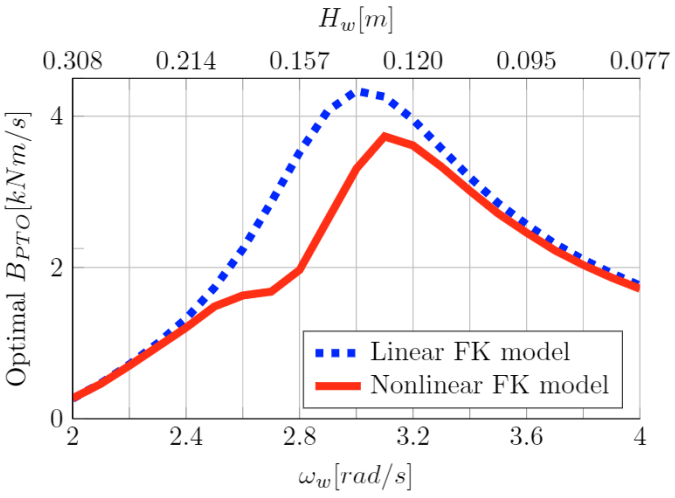

Fig. 1. Optimal power-take off damping coefficient B_{PTO} for each wave condition, according to the linear and nonlinear FK models.

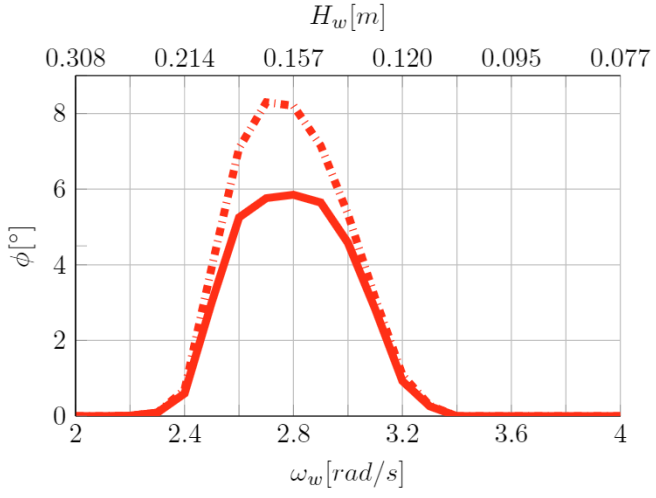

Fig. 2. Maximum roll angle, for each wave condition, according to the nonlinear FK model, using optima computed with the linear (▪▪▪) and nonlinear FK model (—), as shown in Fig. 1.

wave height and wave length, the wave amplitude is chosen so that a constant steepness of 2% is produced, which is at the upper edge of the region of validity of linear Airy's waves. Therefore, the set of analyzed wave conditions is mono-dimensional, with a one-to-one relationship between wave frequency (ω_w) and wave height (H_w).

4. RESULTS

The optimization of a PTO damping coefficient B_{PTO} has been performed for each wave condition. Both the linear FK and the nonlinear FK models are considered, in order to highlight eventual differences in the optimal parameters, and therefore the sensitivity of the controller to modelling errors. The resulting optima are shown in Fig. 1. The two sets of B_{PTO} optima are hereafter referred to as B_L and B_{NL}, indicating which model is used to compute them, either the linear FK model or the nonlinear FK model, respectively.

Significant differences are only found in the range of frequencies between 2.5 and 3rad/s. It is reasonable to infer that such differences are strictly related to parametric resonance in the roll DoF which, as shown in Fig. 2, is generated over the same frequency range.

Obviously, since in the linear FK model there is no excitation mechanism of the roll DoF, the resulting roll motion is inherently zero. On the contrary, in the nonlinear FK model, an internal excitation mechanism is activated, due to parametric resonance, at those frequencies which lead the roll DoF into instability. In Fig. 2, both sets of PTO optima are used, from Fig. 1, obtained using the linear and nonlinear models. A significant dependence on the PTO damping coefficient can be noticed: on the one hand, the larger the PTO damping, the larger the roll response; on the other hand, the frequency range, where parametric roll appears, is overall rather insensitive to B_{PTO}, even though the frequency of the roll peak response changes from 2.8rad/s with lower damping, to 2.7rad/s with higher damping.

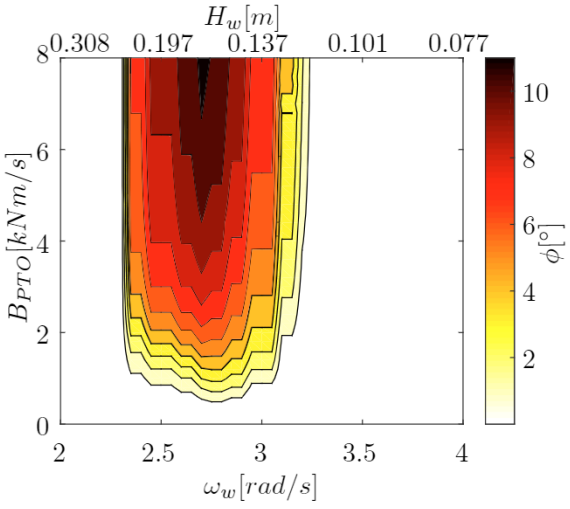

Fig. 3. Sensitivity analysis on the maximum roll angle, for different wave conditions and PTO damping coefficients.

Therefore, it is interesting to undertake a more comprehensive study of the relation between the parametric roll excitation, and the PTO damping coefficients. Figure 3 shows the peak roll response for different wave conditions, and for different B_{PTO} values, ranging from 0 to about twice the maximum optimal PTO value, from Fig. 1. Consistent with Fig. 2, and in agreement with results shown by Tarrant and Meskell (2016), it is found that the parametric roll response significantly increases with B_{PTO}, reaching peaks of 11.3°. Similarly, the frequency range for parametric instability widens as B_{PTO} increases, with the peak frequency for maximum roll motion slightly tending towards larger frequencies. Such behaviour is due to a progressively stiffening system, as the PTO resistance grows (Tarrant and Meskell, 2016).

Figure 3 has important consequences both in the power production region, for the control strategy, and in the survivability mode. In fact, in case of extreme events, a natural tendency to avoid harm to the WEC might be

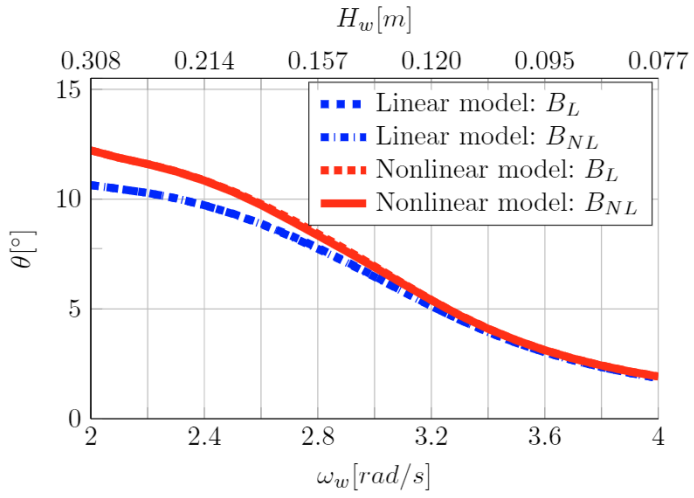

Fig. 4. Maximum pitch angle, for each wave condition, according to the linear and nonlinear FK model, using optima computed with the linear and nonlinear FK model, as shown in Fig. 1.

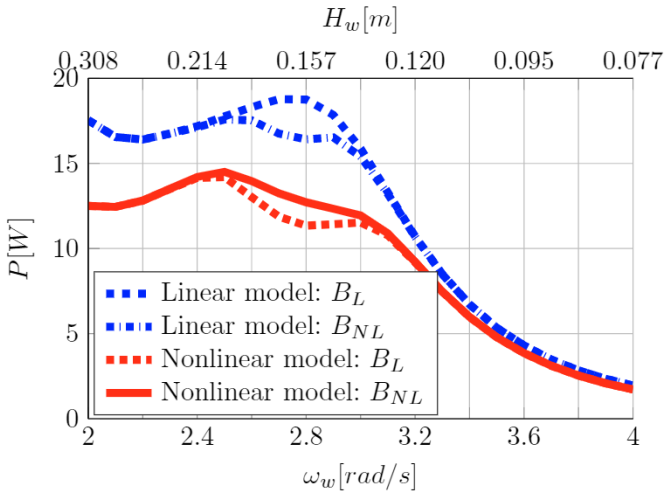

Fig. 5. Power produced, for each wave condition, according to the linear and nonlinear FK model, using optima computed with the linear and nonlinear FK model, as shown in Fig. 1.

to considerably increase the PTO damping, in order to limit the relative motion between the spar and the torus, and avoid end stops striking. However, what Fig. 3 shows is that, for large B_{PTO} values, parametric roll increases further, possibly causing severe structural damage.

Apart from the parametric instability of the roll DoF, the pitch DoF is also parametrically excited. While roll is completely neglected in a linear FK model, pitch is excited in both models. Therefore, Fig. 4 shows the maximum pitch response, using both the linear and nonlinear FK models, each of them using the two sets of PTO damping optima, B_L and B_{NL}, from Fig. 1, for a total of four curves.

Little dependence on the PTO parameters, and consequently on the roll motion, is found, since the curves for each model, using the two sets of B_{PTO}, substantially overlap. In contrast, a significant difference between the two models can be appreciated, with the nonlinear FK model forecasting larger pitch motion, especially at low wave frequencies. The nonlinear FK model is more responsive in pitch, mainly because of the changes in the metacentric height. In particular, the pitch hydrostatic stiffness decreases as the metacentre moves down and, if it eventually falls below the centre of gravity, the restoring force becomes negative, leading to instability (Biran and Pulido, 2013).

Finally, power output prediction, for both linear and nonlinear models, and using the two sets of PTO parameters, is considered, and shown in Fig. 5. Differences within the same model, using different PTO optima, are obviously concentrated in the range of frequencies between 2.5 and 3 rad/s, where parametric roll is excited. Overall, the power produced according to the nonlinear FK model is lower than in the linear FK model, mainly due to the larger pitch motion, as shown in Fig. 4. Indeed, larger differences in power estimation are found at low wave frequencies, where larger errors are obtained in the pitch motion prediction.

The lower efficiency with the nonlinear FK model can be explained with reference to Figs. 2 and 4: roll and pitch motions are both larger in the nonlinear FK model, while the energy of the incoming wave is the same. Therefore, in order to excite such DoFs, and produce larger oscillations, some energy is diverted from the principal (heave) PTO axis, where the energy is harvested, and fed into to the secondary roll/pitch axes, where no PTO conversation takes place. Such a mechanism is particularly evident for parametric roll, and shown in Fig. 6, which presents the envelope of the squared-velocity time traces, for relative heave, and roll motion. Note that the square-velocity is a more representative quantity of the energy absorbed, which is extracted in the relative heave DoF, while wasted in the roll DoF. Figure 6 shows that the energy content in the relative heave motion is larger when the roll motion is still negligible (left part of the time trace); conversely, the gradual increase in parametric roll causes a decrease in relative heave, until steady state is reached (right part of the time trace). Therefore, it is evident that, due to parametric resonance, part of the energy is diverted from relative heave to roll, as schematically represented by the wavy arrow in Fig. 6.

5. CONCLUSIONS

This paper proposes a multi-DoF computationally efficient nonlinear FK model for axisymmetric wave energy devices, and applies it to a simple self-reactive heaving point absorber. The ability to appreciate parametric resonance is demonstrated, which can be detrimental to the device efficiency. It is crucial to highlight how the system response, with particular focus on its nonlinear effects and power production, is highly sensitive to the control parameters. Likewise, the optimization of the control parameters is very dependent on the model fidelity and ability to describe nonlinearities. Therefore, models for control application must be accurate and representative of the complex, nonlinear, system dynamics. Such models also need to be computationally viable, such as the one proposed in this paper, in order to be practically usable in optimization routines.

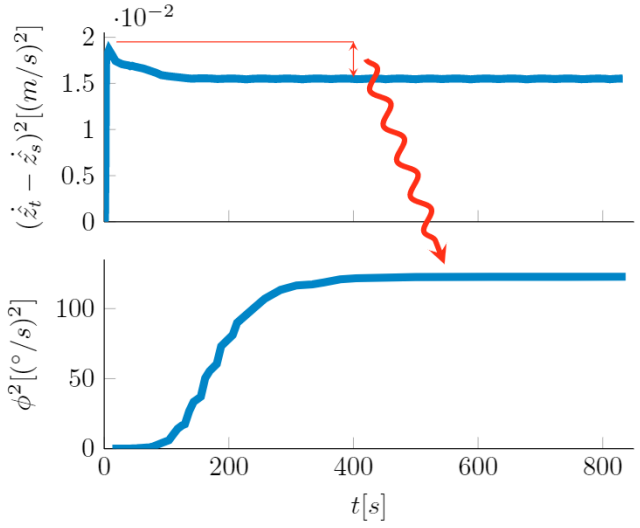

Fig. 6. Envelope of the time traces for the squared-velocity in relative heave (top), and roll (bottom), using the nonlinear optimum at $\omega_w = 2.8 rad/s$. The wavy arrow schematically represents the energy diverted, due to parametric resonance, from the relative heave to the roll DoF.

ACKNOWLEDGEMENTS

This paper is based upon work supported by Science Foundation Ireland under Grant No. 13/IA/1886.

REFERENCES

Babarit, A., Mouslim, H., Clément, A.H., and Laporte-Weywada, P. (2009). On the numerical modelling of the nonlinear behaviour of a wave energy converter. In *Proceedings of the ASME 2009 28th International Conference on Ocean, Offshore and Arctic Engineering, May 31 - June 5*.

Bhinder, M.A., Babarit, A., Gentaz, L., and Ferrant, P. (2011). Assessment of viscous damping via 3d-cfd modelling of a floating wave energy device. In *Proceedings of the 9th European Wave and Tidal Energy Conference, Southampton, UK*.

Biran, A. and Pulido, R.L. (2013). *Ship hydrostatics and stability*. Butterworth-Heinemann.

Davidson, J. and Ringwood, J.V. (2017). Mathematical modelling of mooring systems for wave energy converters - A review. *Energies*, 10(5). doi:10.3390/en10050666.

Faedo, N., Peña-Sanchez, Y., and Ringwood, J.V. (2017). Finite-Order Hydrodynamic Model Determination for Wave Energy Applications Using Moment-Matching. *submitted to Ocean Engineering*.

Falnes, J. (2002). *Ocean waves and oscillating systems*. Cambridge University Press.

Fossen, T.I. (2011). *Handbook of marine craft hydrodynamics and motion control*. John Wiley & Sons.

Fossen, T.I. and Nijmeijer, H. (2012). *Parametric resonance in dynamical systems*. Springer.

Gilloteaux, J.C. (2007). *Mouvements de grande amplitude d'un corps flottant en fluide parfait. Application á la recuperation de l'energie des vagues*. Ph.D. thesis, Ecole Centrale de Nantes-ECN.

Giorgi, G. and Ringwood, J.V. (2016). Implementation of latching control in a numerical wave tank with regular waves. *Journal of Ocean Engineering and Marine Energy*, 2(2), 211–226.

Giorgi, G. and Ringwood, J.V. (2017). Froude-Krylov and Viscous Drag Representations in Nonlinear Wave Energy Devices Models in the Computation/Fidelity Continuum. *Ocean Engineering*, 141, 164–175.

Giorgi, G. and Ringwood, J.V. (2018a). A Compact 6-DoF Nonlinear Wave Energy Device Model for Power Assessment. *IEEE Transactions on Sustainable Energy*. doi:10.1109/TSTE.2018.2826578.

Giorgi, G. and Ringwood, J.V. (2018b). Analytical Formulation of Nonlinear Froude-Krylov Forces for Surging-Heaving-Pitching Point Absorbers. In *ASME 2018 37th International Conference on Ocean, Offshore and Arctic Engineering*.

Giorgi, G. and Ringwood, J.V. (2018c). Relevance of pressure field accuracy for nonlinear FroudeKrylov force calculations for wave energy devices. *Journal of Ocean Engineering and Marine Energy*, 4(1), 1–15. doi: 10.1007/s40722-017-0107-5.

Penalba, M., Mérigaud, A., Gilloteaux, J.C., and Ringwood, J.V. (2017). Influence of nonlinear FroudeKrylov forces on the performance of two wave energy points absorbers. *Journal of Ocean Engineering and Marine Energy*, 3(3), 209–220. doi:10.1007/s40722-017-0082-x.

Tarrant, K.R. and Meskell, C. (2016). Investigation on parametrically excited motions of point absorbers in regular waves. *Ocean Engineering*. doi: 10.1016/j.oceaneng.2015.10.041.

Wendt, F.F., Yu, Y.H., Nielsen, K., Ruehl, K., Bunnik, T., Touzon, I., Nam, B.W., Kim, J.S., Kim, K.H., and Janson, C.E. (2017). International Energy Agency Ocean Energy Systems Task 10 Wave Energy Converter Modeling Verification and Validation. In *12th European Wave and Tidal Energy Conference*. Technical Committee of the European Wave and Tidal Energy Conference.